九州大学学術情報リポジトリ
Kyushu University Institutional Repository

Variations in slice sensitivity profile for various height settings in tomosynthesis imaging: Phantom study

倉本, 卓

https://doi.org/10.15017/2534386

出版情報：Kyushu University, 2019, 博士（保健学）, 課程博士
バージョン：
権利関係：

KYUSHU UNIVERSITY

Physica Medica 53 (2018) 108–117

Contents lists available at ScienceDirect

Physica Medica

journal homepage: www.elsevier.com/locate/ejmp

Original paper

Variations in slice sensitivity profile for various height settings in tomosynthesis imaging: Phantom study

Taku Kuramoto[a,b,*], Junji Morishita[c], Toyoyuki Kato[b], Yasuhiko Nakamura[d]

[a] Department of Health Sciences, Graduate School of Medical Sciences, Kyushu University, 3-1-1 Maidashi, Higashi-ku, Fukuoka 812-8582, Japan
[b] Division of Radiology, Department of Medical Technology, Kyushu University Hospital, 3-1-1 Maidashi, Higashi-ku, Fukuoka 812-8582, Japan
[c] Department of Health Sciences, Faculty of Medical Sciences, Kyushu University, 3-1-1 Maidashi, Higashi-ku, Fukuoka 812-8582, Japan
[d] Department of Radiological Science, Faculty of Health Sciences, Junshin Gakuen University, 1-1-1, Chikushigaoka, Minami-ku, Fukuoka 815-8510, Japan

ARTICLE INFO

Keywords:
Tomosynthesis imaging
Slice sensitivity profile
Slice thickness
Center of rotation

ABSTRACT

Understanding the properties of slice sensitivity profile (SSP), or slice thickness, is crucial for an accurate and highly reproducible diagnosis using tomosynthesis imaging. The objectives of the present study are therefore to quantitatively evaluate how the SSP with the use of a small metal bead is affected by different settings of the height from the table and the height of the center of rotation (COR) in tomosynthesis imaging except for the digital breast tomosynthesis, and visually verify the effects on tomosynthesis images. The reconstruction filters used were three types of filtered back-projection and iterative reconstructions. The SSP was measured from the full width at half maximum (FWHM-SSP) of the profile curve of the bead in the perpendicular direction (z direction) relative to the table. Two types of anthropomorphic phantoms simulating the human body, with bones and soft tissues, were used to study the effects of different settings for the COR height. In all reconstruction filters, the FWHM-SSP changed as the height of the bead varied when the bead and COR were set to the same height from the table. If the bead and the COR were set to different heights, the FWHM-SSP increased (decreased) when the height of the bead was set to be greater (less) than the height of the COR. These changes were also confirmed on the anthropomorphic phantom images of the bones and soft tissues.

1. Introduction

Tomosynthesis imaging is a digital tomograpic technology [1] that enables the acquisition of tomographic images of three-dimensional anatomical structures in the human body with the focal point aligned to any plane chosen that is parallel to an examination table. It was first reported in 1972 by Grant [2], as an improvement to the conventional tomographic technique reported by Plantes in the 1930s [3]. Since entering the 1990s, technical innovations and the development of flat panel detector (FPD) enabled the investigation of full-fledged clinical applications of tomosynthesis imaging. Currently, general radiography devices, x-ray fluoroscopic imaging system, and mammography devices that are capable of tomosynthesis imaging have been introduced in many facilities [4]. Tomography with conventional x-ray film can only acquire a tomographic image of one slice at a time; if tomographic images of multiple slices are needed for examination, it is then necessary to either use simultaneous multisection tomography—where images are captured with x-ray intensifying screens and x-ray films layered over one another—or to capture x-ray images multiple times with different tomographic planes. With tomosynthesis imaging, however, tomographic images of multiple different slices can be obtained in a single scan, centered on any height chosen from the table. The advantages include lower patient radiation doses compared to computed tomography (CT) [5,6], and the ability to better mitigate the effects of metal artifacts than with CT or magnetic resonance imaging (MRI). Tomosynthesis has been described as useful in reports on many different aspects, such as mammography [7–9], chest imaging [10–13], orthopedic surgery [14–19], and radiation treatment planning [20].

Tomosynthesis imaging entails imaging while simultaneously moving the x-ray tube and x-ray detector in opposite directions. The point that forms the center of the angular range, which is formed between the start and end points of irradiation with the x-ray tube and x-ray detector, is called the center of rotation (COR). Although the height of the anatomical structure of interest is already known prior to examination, imaging is preferably performed with the COR set to that height [21]. For example, when tomographic images of the lumbar

* Corresponding author at: Division of Radiology, Department of Medical Technology, Kyushu University Hospital, 3-1-1 Maidashi, Higashi-ku, Fukuoka 812-8582, Japan.
E-mail addresses: t.kura13@gmail.com, kuramoto@r-tec.med.kyushu-u.ac.jp (T. Kuramoto).

https://doi.org/10.1016/j.ejmp.2018.08.009
Received 11 April 2018; Received in revised form 14 July 2018; Accepted 12 August 2018
Available online 23 August 2018
1120-1797/ © 2018 Associazione Italiana di Fisica Medica. Published by Elsevier Ltd. All rights reserved.

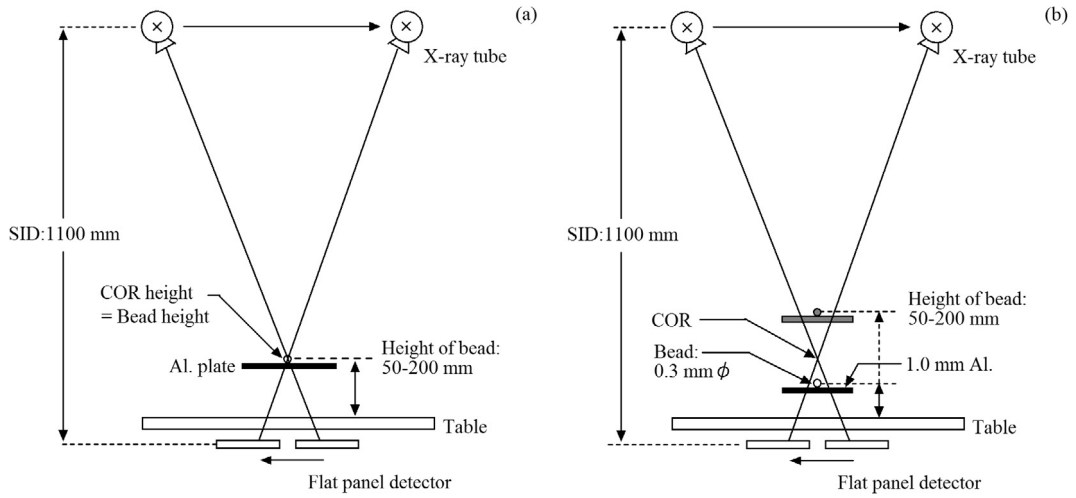

Fig. 1. Geometry for data acquisition in case of (a) the height of the bead match the COR and (b) the height of the bead in the image do not coincide with the COR.

spine or sternum are to be captured from a patient in the supine position on the table, the COR is set to 5 cm or 15 cm, corresponding to the respective heights from the back from the table. If, however, the height from the back where an anatomical structure is located is not known, or if multiple regions of interest with different heights exist, then it is clinical practice to set the COR to a height that is half of the thickness of the subject. Tomosynthesis imaging thus offers the ability to acquire tomographic images of anatomical structures at the same height as the COR, or even of slices of a different height from the COR.

The slice sensitivity profile (SSP) is often used to describe a system's resolving power in the perpendicular direction with respect to the reconstructed planes (z resolution), and the full width at half maximum of SSP (FWHM-SSP) is evaluated as the slice thickness. Although the SSP is one of the most important image quality metrics for tomosynthesis, cautious investigation is required for this analysis. In theory, the SSP can be measured via imaging a small metal bead whose size is significantly smaller than the slice thickness of the acquisition system [24]. The previous study evaluated the SSP using a small bead with 0.3 mm in diameter [30]. Moreover, the structures at other depths (out-of-focus) generate artifacts in the different reconstructed planes owing to the limited angular range and number of projections in tomosynthesis imaging. Several studies have been evaluated regarding this type of artifacts using artifact spread function (ASF) [22–26].

In the digital breast tomosynthesis (DBT) systems, the most comprehensive quality assurance (QA) and a quality control (QC) protocol has recently been proposed by the European Reference Organisation for Quality Assured Breast Screening and Diagnostic Services (EUREF) [27]. Moreover, specific QC protocols for DBT have been reported in different screening programs [28,29]. In these reports, the image quality factors such as the SSP and the ASF had been evaluated in DBT. However, there are no specific guidelines for QA and QC in chest and bone tomosynthesis that is provided in general radiography and/or fluoroscopic imaging systems. In addition, the geometry of motion of the x-ray tube and/or detector is different between DBT system and general radiography and/or fluoroscopic imaging system. Therefore, it is necessary to evaluate the image quality even in these systems other than the DBT system.

The SSP in tomosynthesis imaging depends on not only on the angular range but also on the image reconstruction algorithm. An accurate knowledge of the properties of the z resolution is significant because radiological technologists have to set the optimal conditions such as setting the COR and selecting the image reconstruction algorithm for the imaging. It is also important that the clinical radiologists interpreting the images should understand the properties of the z resolution for the imaging. Understanding the z resolution is therefore important from the point of view of the radiological technologists as well as administrators who operate the system. In previous studies regarding evaluating the z resolution in tomosynthesis imaging [23–26,30], the SSP was measured with the height of the COR set to match the height from the table. To our knowledge, none have reported studies regarding the SSP in various combinations from the height of the table and the height of the COR. Moreover, no investigation regarding the z resolution or slice thickness has been reported using anthropomorphic phantom that approximates clinical practice.

The objectives of the present study are therefore to quantitatively evaluate how the SSP with the use of a small metal bead is affected by different settings of the height from the table and the height of the COR in tomosynthesis imaging except for DBT, and visually verify the effects on tomosynthesis images. We used anthropomorphic phantoms for chest and bones (orthopedic area) for evaluating tomosynthesis imaging except for breast imaging.

2. Materials and methods

2.1. Image acquisition

The tomosynthesis imaging system used was the SONIALVISION G4 (Shimadzu Corporation, Kyoto, Japan), which can acquire two-dimensional projected digital radiographic images, fluoroscopic images, and tomosynthesis images. The x-ray detector was a cesium iodide indirect conversion-type FPD, with a pixel size, effective number of pixels, and detector surface area of 0.139×0.139, 2880×2880, and $432 \times 432\,mm^2$, respectively. The pixel size of the tomosynthesis image is $0.278 \times 0.278\,mm^2$, owing to pixel binning during image reconstruction. The source-to-image receptor distance (SID) of the tomosynthesis imaging is 1100 mm. The angular range used for the tomosynthesis imaging was 40°—which is commonly used in clinical practice (such as head, thoracoabdominal, or limb images)—as well as 20° in some of the experiments. The projection time for acquiring the tomosynthesis images is approximately 5 s, for both angular ranges of 40° and 20°. A stainless-steel bead (simply called “the bead” hereafter) with a diameter of 0.3 mm was used to measure the SSP of tomosynthesis images. Fig. 1 and Table 1 show the geometric arrangement and acquisition parameters, respectively, for acquiring the tomosynthesis images.

The SSP of tomosynthesis image was evaluated by measuring the SSP with the same height as that of the COR, modified within a range of 50 mm–200 mm over the table (Fig. 1(a)), and with the COR and bead set to different heights (Fig. 1(b)). In these experiments, the bead height was changed 50 mm at a time, and the measurements taken with the

Table 1
Acquisition parameters for tomosynthesis imaging.

Parameters	Conditions	
Exposure	60 kV, 2.0 mA·s (250 mA, 8 msec.)	
Acquisition time	5 s	
Acquisition images	74	
Angular range	40° (±20°)	
Flame rate	15 fps	
Source to image receptor distance (SID)	1100 mm	
Grid	Ratio: 10:1, Focus distance: 120 cm, Lines/Inch: 50 line/cm, Interspace material: Al.	
Field of view	9 inch	
Height of the bead position	50-200 mm	
Height of the COR	50-250 mm	
Reconstruction slice interval	0.5 mm	
Reconstruction filters	FBP	Low-pass filter
		High-pass filter
		Moderate bandwidth filter
	IR	IR filter

FBP: filtered back projection, IR: iterative reconstruction.

Table 2
Combination of bead height from examination table and CORs.

Height of bead (mm)	Height of center of rotation (COR) (mm)
50	50, 100, 150
100	100, 150, 200
150	100, 150, 200, 250
200	150, 200, 250

combinations of bead and COR heights are shown in Table 2. The reconstruction filters were used three types of filtered back projection (FBP) ((low-pass filter (LPF), high-pass filter (HPF), and moderate bandwidth filter (MBF)) and iterative reconstruction (IR). Types of FBPs are HPF, MBF, and LPF as shown in Fig. 2. If we change the type of FBPs, the degree of occurrence of the ghost artifact will change based on the upper limit of the frequency band [30]. The IR provided by the manufacturer was used in this study (called Normal in this system). This filter did not include a process of metal extraction to reduce the metal artifacts. In the IR, the number of iterations was set to 4, which is used in majority of the clinical practices for this tomosynthesis system. For both FBP and IR, the slice interval as an index in image reconstruction was set at 0.5 mm, which is the minimum setting of the system used in this study.

2.2. Evaluation of slice sensitivity profile

The images acquired by tomosynthesis imaging were transferred to a personal computer, where the general purpose image analysis software (ImageJ (NIH, Bethesda, MD)) was used to measure the SSP from the full width at half maximum (FWHM) of the profile curve of the bead in the perpendicular direction (z direction) relative to the table, which was parallel to the floor of the laboratory. Fig. 3 shows the procedure for image analysis. The digital profile was acquired from the digital value of the bead central coordinate in the z direction relative to the table. We defined this digital profile as the slice sensitivity profile (SSP). The FWHM of SSP (FWHM-SSP) was used for evaluation of the z resolution.

The SSP was measured with four types of reconstruction filters at an angular range of 40°. All measurements were repeated five times on the same day, with the mean values taken as the representative value for each of the conditions. In order to confirm the reproducibility of the measurement, the same measurement was carried out on another day. Further, the rate of change in the SSP relative to the change in COR was calculated with reference to the value for when the heights of the bead and the COR matched. To also investigate the effects at an angular range of 20°, an HPF was used to measure the SSP, and this was compared with the result of the 40° angular range.

2.3. Evaluation of artifact spread function (ASF)

The artifact ASF [22,23] was calculated using a 0.3 mm bead in diameter to evaluate the effects of blur in the z direction as shown in Eq. (1).

$$ASF(z) = \frac{PV_{max}(Z) - PV_{bg}(Z)}{PV_{max}(Z_0) - PV_{bg}(Z_0)} \quad (1)$$

where z_0 is the position of in-focus plane of the bead, z is the position of the off-focus plane, PV_{max} is the maximum value of the bead in that plane, and PV_{bg} is the mean pixel intensity of the image background, respectively. PV_{bg} is the mean pixel value averaged over two 5 × 5 pixel regions of interest located in the background that is not affected by tube movement, with a center-to-center distance of 25 pixels to the bead. All measurements were repeated five times, and the mean value was used as the representative value.

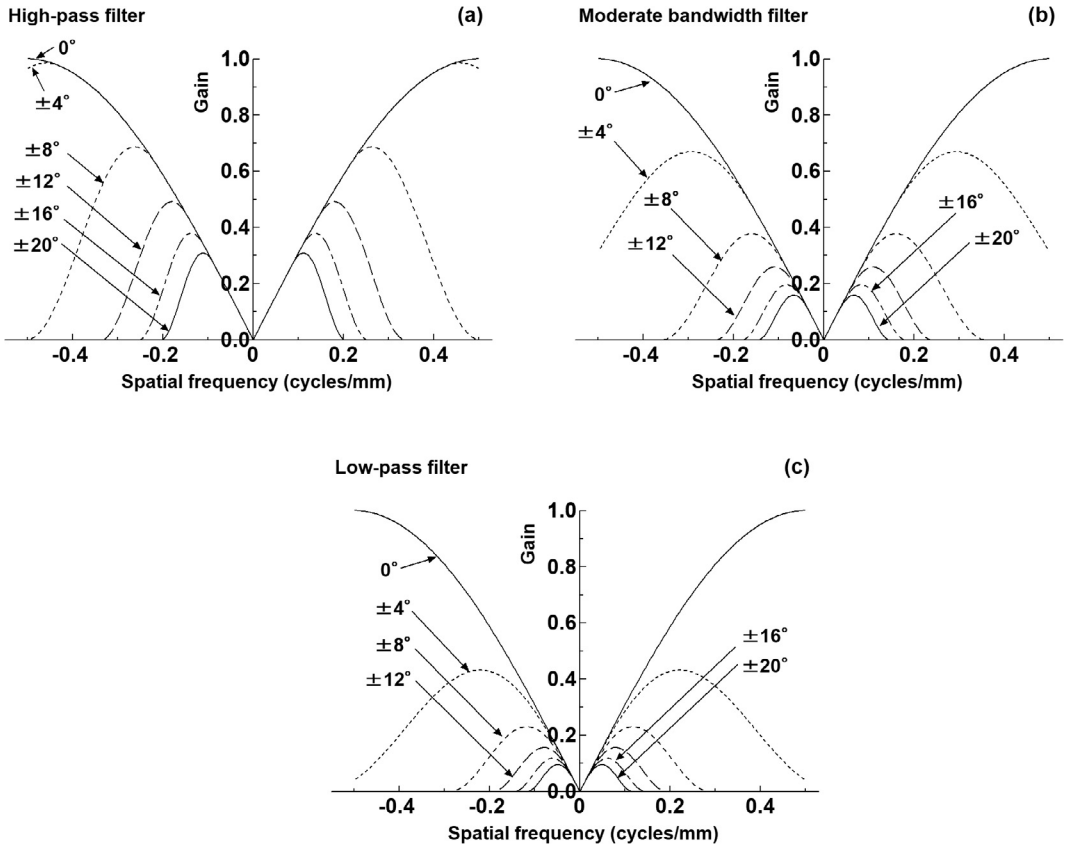

Fig. 2. Shapes of the FBP reconstruction filters for high-pass filter (a), moderate bandwidth filter (b), and low-pass filter (c).

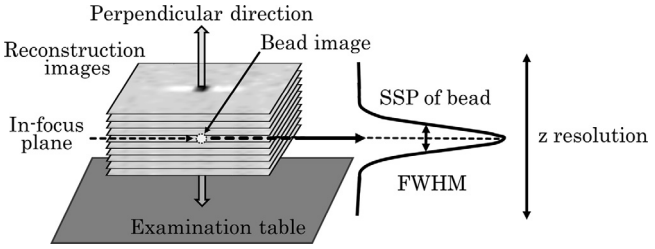

Fig. 3. SSP measured from the digital value of the bead in the perpendicular direction (z direction) relative to the table.

2.4. Influence of the phantom images

To verify changes in the SSP on the images obtained by tomosynthesis imaging, we used a wrist phantom (PB-10; Kyoto Kagaku, Kyoto, Japan) for the bone tissue assessment, and a phantom prepared by layering scattering plates onto the front surface and rear surface of a chest phantom (Chest Phantom N1, Chest plates; Kyoto Kagaku, Kyoto, Japan) for the soft tissue assessment. The wrist phantom had a stainless-steel bead with a diameter of 0.3 mm (called a positioning bead hereafter) arranged on the lateral surface of the ulna at a height half the thickness of the phantom. The positioning bead was adhered to the side of the phantoms to evaluate the images of slices at different heights and at the same height as the COR. The wrist phantom was placed on polystyrene foam with a height of 120 mm placed on the table. In this case, the positioning beads adhered to the side of the phantom were located at a height of 150 mm from the table. The chest phantom, meanwhile, is approximately 300 mm thick including the scattering plates, and thus the phantom was placed directly on the table, with the positioning bead affixed to the right-side surface of the phantom at a height of 150 mm from the examination table, which is approximately half the height of the phantom. The slice where the positioning bead was most distinctly rendered was selected from the multiple tomosynthesis images acquired, and the images were studied. The two phantoms were imaged to obtain tomosynthesis images with the COR set to three different heights: 100, 150, and 250 mm. The wrist and chest phantoms were imaged under conditions of tube voltage: 50 kV and 120 kV, and tube current–time product: 1.25 mA·s and 0.8 mA·s, respectively, with angular range 40°. Other acquisition parameters (acquisition time, acquisition images, frame rate, SID, and grid) are the same as shown in Table 1. The reconstruction filters used from among the FBP reconstruction filters were the HPF for the wrist phantom and the LPF for the chest phantom, taking the actual clinical practice into consideration.

2.5. Influence of the magnification rate of the bead

The magnification rate (MAG) of a bead being used to measure the FWHM-SSP in images obtained by tomosynthesis imaging changes if a change to the height of the bead from the table occurs. We therefore investigated the relationship between the FWHM-SSP and MAG where the bead and the COR were set to the same height.

2.6. Influence of the apparent angle for the bead

The angular range of the tomosynthesis imaging system used is defined as the angle to which the x-ray tube is moved to capture images, with the height of the COR as the origin point. If the COR height is different from the height of the bead being used to evaluate the SSP, then the angular range as seen from the bead (called the “apparent angular range” hereafter) will be different from the set angular range. The apparent angular range of the bead is thought to affect the SSP, because the apparent angular range changes with the settings for the COR and bead heights. We therefore examined the relationship between

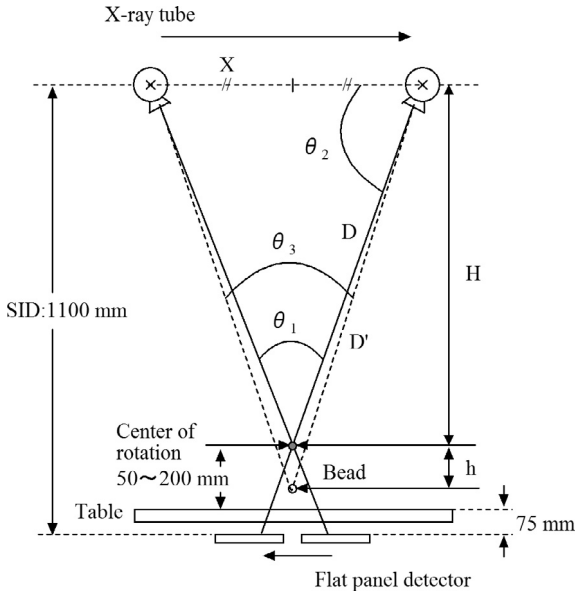

Fig. 4. Geometry for calculating the apparent angle for the bead.

the COR height setting and the apparent angular range for when the COR height differs from the height used to evaluate the SSP (Fig. 4).

3. Results

Certain analyzed bead images regarding the SSP evaluation with LPF, when the bead and the COR were set to the same height from the table, are shown in Fig. 5, and the SSP obtained from these images is shown in Fig. 6. The bead image of the height of the table with 50 mm was visible further from the in-focus plane compared with other heights (Fig. 5). These trends were also confirmed in all filters and various height settings of the beads. Moreover, Fig. 7 shows the change in the FWHM-SSP for tomosynthesis imaging obtained with the four types of reconstruction filters when the bead and the COR were set to the same height from the table. The error bars in the graph show the standard deviation of the measured values. For each condition, the measured values exhibited high reproducibility (coefficient of variation < 0.07). When the bead of the same height as the height of the COR was increased, the FWHM-SSP tends to decrease slightly with FBP. With IR,

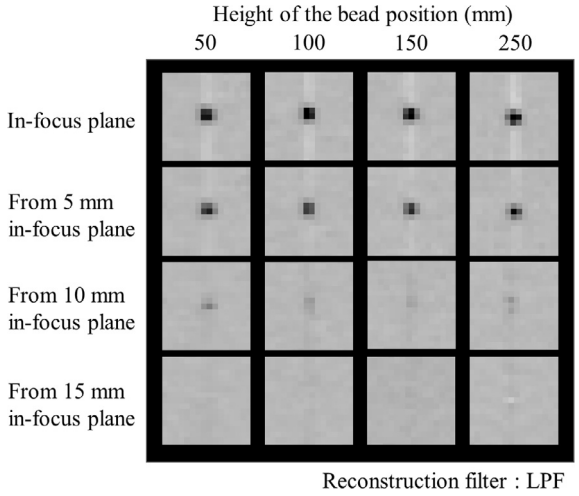

Fig. 5. Bead images for evaluation the SSP. The height of the bead matched the height of the COR for LPF were shown in these figures. First column is in-focus plane; second column is 5 mm from in-focus plane; third column is 10 mm from in-focus plane; fourth column is 15 mm from in-focus plane.

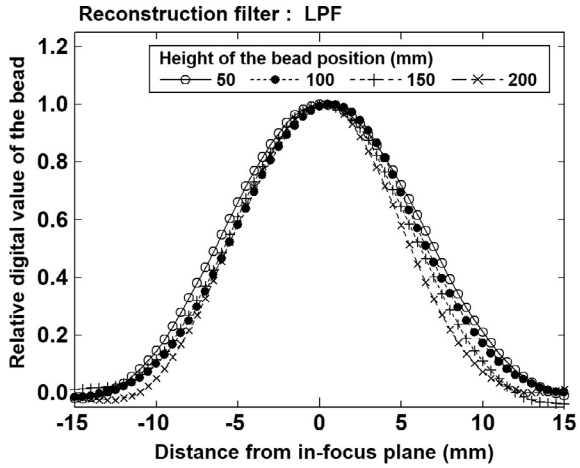

Fig. 6. SSPs obtained from the bead image were shown in Fig. 5 for LPF. The height of the bead matched the height of the COR.

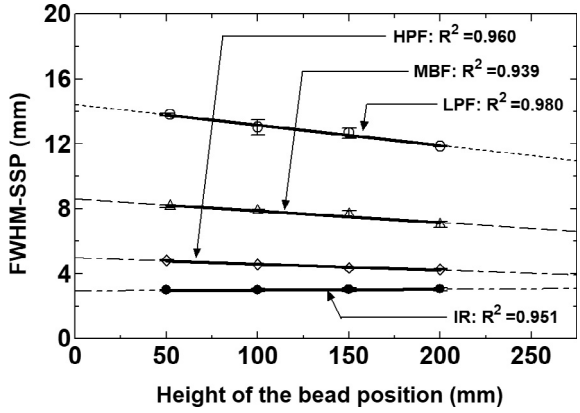

Fig. 7. Changes in the FWHM-SSPs with different FBP and the IR filters. The height of the bead matched the height of the COR.

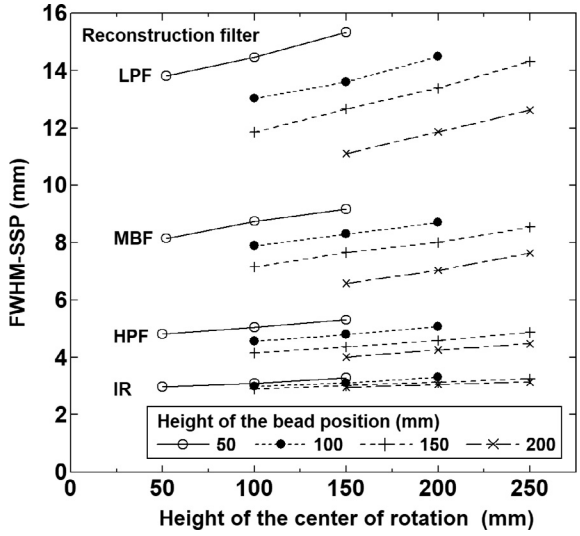

Fig. 8. Relationships between various heights of the center of rotation and the FWHM-SSP in different bead position from table. Bead position differ from the COR.

however, the FWHM-SSP did not change significantly even when the bead (COR) height was increased.

Fig. 8 shows the change in the FWHM-SSP when the bead and the COR were set to different heights. The FWHM-SSP increased with all

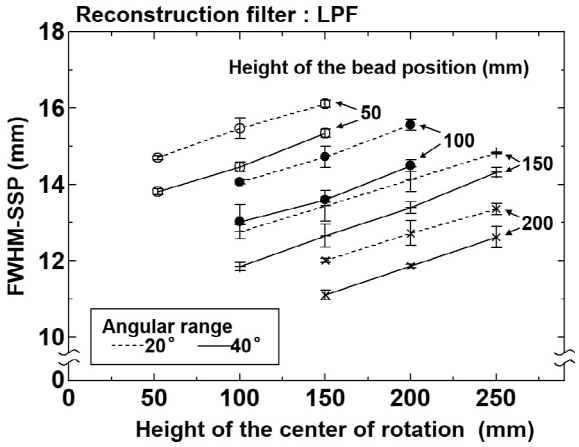

Fig. 9. Comparison of the FWHM-SSP for 20 and 40° using the LPF. Relationships between various heights of the center of rotation and the FWHM-SSP in different bead position from table. Bead position differs from the COR. Results in LPF are shown in this figure.

reconstruction filters whenever the height of the COR was set to be greater than the height of the bead. When the height of the COR was set to be less than the height of the bead, however, the FWHM-SSP decreased. The rate of change in the FWHM-SSP when each FBP was used increased (/decreased) via a proportion of approximately 5% when the height of the COR became larger (/smaller) than the spatial position of the bead in 50 mm increments, tested in our study. The rate of change in the FWHM-SSP when IR was used did not increase as much as with FBP.

Fig. 9 shows the measurement results for the FWHM-SSP with 20° and 40° angular range using the LPF. In all of the combinations of bead and COR height settings used in the present study, the angular range of 20° had greater FWHM-SSP than with 40°. Table 3 shows the rate of change in the FWHM-SSP according to the combination of bead and COR height with an angular range of 20°. The rate of change in the FWHM-SSP increased (/decreased) by a proportion of approximately 5% when the COR became higher (/lower) than the spatial position of the bead in 50 mm increments, similar to with 40°.

The relationship between the ASF and the various height settings were investigated via comparing the ASF with respect to different filters. Certain representative ASF curves with LPF are shown in Fig. 10. Fig. 10(a) shows the variation in the ASF curves in case of the high position of the bead from the table and the COR is set to the same height. Further, Fig. 10(b) shows the results in the case when the height of bead was set at 150 mm and the height of the bead was different from the COR. When the height of COR and the bead was higher from (or near to) the table, the ASF tends to be narrower (or wider). Moreover, the FWHM of the ASF (hereafter referred to as “FWHM-ASF”) at various heights of the bead position and COR with regard to LPF is shown in Fig. 11. The FWHM-ASF increased whenever the height of the COR was set to be greater than that of the bead. When the height of the COR was set to be less than that of the bead, however, the FWHM-ASF decreased. These trends were also confirmed for all filters and at various height settings of the bead.

Figs. 12 and 13 show the tomosynthesis imaging for the wrist and chest phantoms with the positioning bead, respectively, having been arranged on the human body phantom, at a height of 150 mm from the table and by changing the COR height to 100, 150, and 250 mm. Table 4 shows the FWHM-SSP measured with different reconstruction filters when the bead for the FWHM-SSP measurement was arranged at a height of 150 mm from the table and the COR height was changed. The tomosynthesis imaging of the wrist phantom shown in Fig. 12 shows that when the low (Fig. 12(a)) and high (Fig. 12(c)) COR height settings are compared, a larger COR height resulted in the more extensive rendering of the thumb side of the scaphoid bone. We also observed that as the COR height increased, the more the pisiform bone was rendered on the superior side of the triquetral bone. The difference in the FWHM-SSP between the two images acquired with the LPF (Fig. 12(a) and (c)) is 0.71 mm (Table 4). The tomosynthesis images of the chest phantom (Fig. 13) show that a higher COR height setting allows for a clearer observation as far as the peripheral tracheal branches of the right superior lobar branch of the lung. When the tracheal branches, indicated with the arrow, are observed, they are essentially not rendered with a low COR height; however, as the COR height increases, they become more clearly distinguishable. The difference in the FWHM-SSP between the two images shown in Fig. 13(a) and (c) acquired with the MPF is 1.39 mm (Table 4). The difference in the FWHM-SSP actually measured from tomosynthesis imaging and the difference in visual rendering with tomosynthesis imaging of the wrist and chest phantoms nearly match.

Table 5 shows the MAG and the FWHM-SSP measured with different filters for when the bead and COR were set to the same height. As the bead drew higher from (closer to) the table, the MAG would increase (decrease). In the FBP used, the value of the product of the “FWHM-SSP” and “MAG” at each bead height is close to a constant value, and is within 5% when compared with the value at a bead height of 50 mm as a reference. In the IR case, the greater the bead height, the greater is the value of the product of the “FWHM-SSP” and “MAG” at each bead height.

Fig. 14 shows the relationship between the COR height setting and the apparent angular range of the bead. When the bead was arranged lower than the COR height, the apparent angular range of the bead was less than the angular range set forth for the COR (40°); however, when the bead was arranged higher than the COR height, the angular range of the bead was greater. With each 50 mm increase (decrease) in the bead height from the COR, the apparent angular range decreased (increased) in 2° increments. At all bead heights, the apparent angular range of the bead and the COR height had a negative correlation, and exhibited a constant rate of change.

Table 3
Comparisons of the changing rates in various height settings. The height of the bead match the height of COR, and low-pass filter and 20° in angular ranges were used for this measurements. The changing rate of the FWHM-SSP for various bead positions increased (or decreased) at the rate of about 5% as the height of COR increased (or decreased) every 50 mm.

Height of COR (mm)	Low-pass filter Bead height (mm)			
	50	100	150	200
50	1.000	…	…	…
100	1.052	1.000	0.949	…
150	1.096	1.047	1.000	0.944
200	…	1.106	1.051	1.000
250	…	…	1.103	1.050

4. Discussion

We measured the SSP in tomosynthesis imaging in cases where the height used for evaluation (i.e., the bead height) did and did not match the COR height, and confirmed our findings with phantom images.

In the reconstruction filters used in this study, the change in the SSP was found to differ between the FBP and IR both when the height from the table to the bead and the COR were set to the same height, and when the height set for the bead was different from the COR. This may be due to the different principles behind the methods of reconstruction with FBP and IR. The three types of FBPs have different levels of high-frequency low-pass restrictions (Fig. 2). Meanwhile, the inbuilt IR algorithm has not been made accessible to users by the manufacturer. However, that used in this study is presumed to be based on ordered

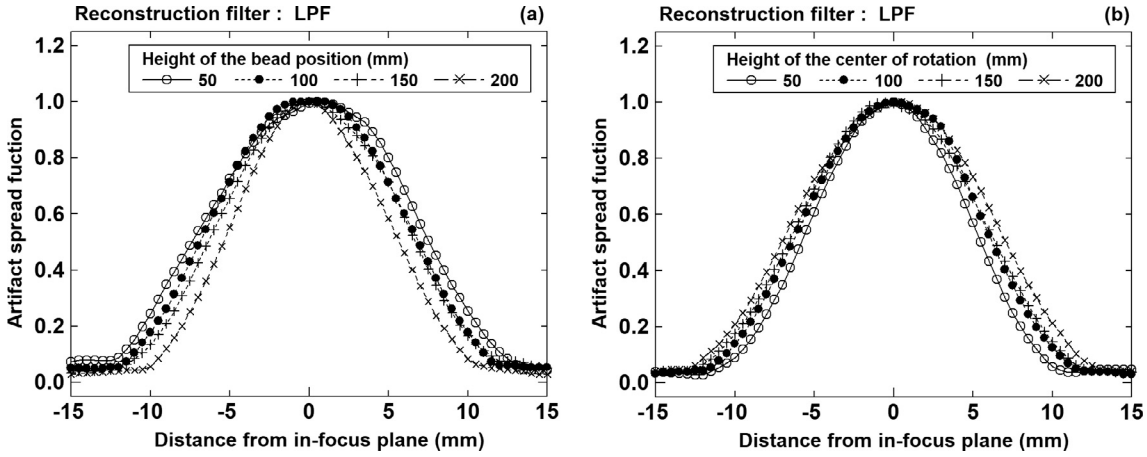

Fig. 10. ASF curves for LPF: (a) the height of the bead matched the height of the COR; (b) in the case when the height of bead was set at 150 mm and the height setting for the bead was different from the COR.

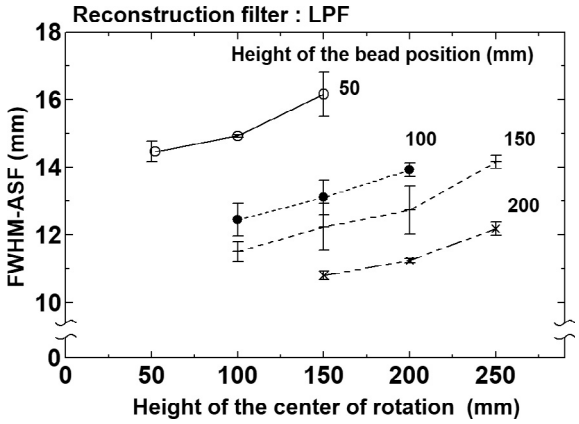

Fig. 11. FWHM-ASF at various heights of the bead position and COR from the table with respect to LPF. Each FWHM-ASF was averaged based on results obtained in five measurements. The error bars in the graph indicate the standard deviation.

subset-expectation maximization (OS-EM) described in the previous research [33]. An initial image is assumed and the concordance between a projection created by calculations from this image and an actually measured projection is increased by iterative calculation; the IR of the manufacturer used here is thus thought to have properties that considerably reduce the metal artifacts [19]. This is thought to have restricted the appearance of the bead reflected in the slices up and down directions from the height of the bead, which is arranged to measure the SSP. When the heights of the bead and COR increased, the value of the product of the "FWHM-SSP" and "magnification rate at each bead height" increased, but the change exhibited was less than that of the magnification rate. In other words, using the IR is believed to have reduced the effects of the magnification rate of the bead on the SSP, thus exhibiting a different trend from FBP.

The images (Figs. 12 and 13) captured with two types of FBP reconstruction filters (LPF and MPF) under conditions where the heights of the centers of the two different anthropomorphic phantoms were set to 150 mm also allowed for the visual confirmation that when the COR height setting is different, the z resolution is different even when the same subject is imaged at the same height from the table. In the present study, these effects were confirmed by using anthropomorphic phantom with bones and soft tissues approximating the tissues in the human body; thus, similar results would be shown with an actual human body.

With FBP, the FWHM-SSPs were decreased when the bead position is increased as the height of the bead matches the COR. The reason is related to the change in the bead distance from the FPD. As the position of the bead increases, the distance between the FPD and the bead becomes large. Therefore, the signal value of the bead image in the projection data attenuates owing to x-ray attenuation in the air. As a result, in the reconstructed images with FBP, the bead image propagation was reduced in other depths (the out-of-plane), and the FWHM-SSP was decreased. Moreover, the value of the product of the "FWHM-SSP" and

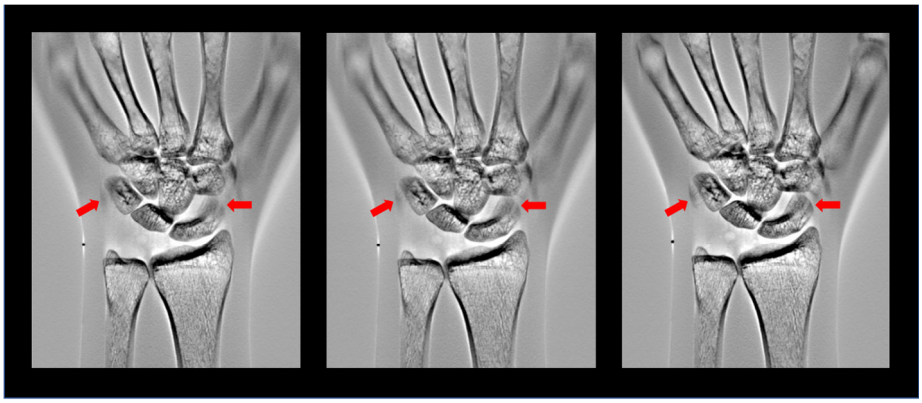

(a) COR 100 mm (b) COR 150 mm (c) COR 250 mm

Fig. 12. Comparison of the wrist phantom's images obtained with various height of the COR. The height of phantom from the table was same height in all images. The reconstruction filters used from among the FBP reconstruction filters were the HPF for the wrist phantom.

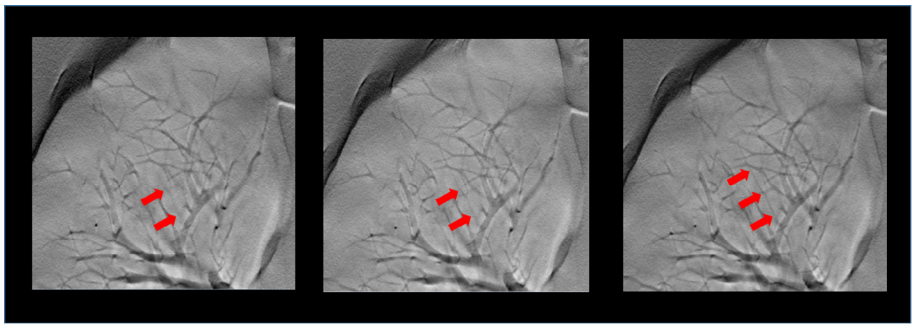

(a) COR 100 mm (b) COR 150 mm (c) COR 250 mm

Fig. 13. Comparison of the chest phantom's images obtained with various height of the COR. The height of phantom from the table was same height in all images. These were enlarged images of the right upper lobe branches of the chest phantom. The reconstruction filters used from among the FBP reconstruction filters were the LPF for the chest phantom.

Table 4
FWHM-SSP measured at different CORs for two reconstruction filters. The reason for choice of MPF and HPF is based on clinical usage in chest and bone imaging.

Reconstruction filter	Height of COR (mm)	FWHM-SSP (mm)
HPF	100	4.16
	150	4.36
	250	4.87
MPF	100	7.15
	150	7.66
	250	8.54

Table 5
Relationship between the FWHM-SSP and the magnification rate at the height of the bead in each reconstruction filters. The ratio of FWHM-SSP were calculated based on the FWHM-SSP at 50 mm in each filter.

Reconstruction filter	The height of the bead (mm)	50	100	150	200
	Magnification rate of bead (MAG)	1.13	1.19	1.26	1.33
HPF	$FWHM\text{-}SSP_{HPF}$ (mm)	4.82	4.56	4.36	4.26
	MAG × $FWHM\text{-}SSP_{HPF}$	5.44	5.42	5.48	5.68
	Ratio	1	0.997	1.008	1.045
MBF	$FWHM\text{-}SSP_{MBF}$ (mm)	8.15	7.89	7.66	7.04
	MAG × $FWHM\text{-}SSP_{MBF}$	9.19	9.38	9.63	9.38
	Ratio	1	1.020	1.047	1.020
LPF	$FWHM\text{-}SSP_{LPF}$ (mm)	13.81	13.03	12.66	11.86
	MAG × $FWHM\text{-}SSP_{LPF}$	15.58	15.49	15.92	15.82
	Ratio	1	0.994	1.021	1.015
IR	$FWHM\text{-}SSP_{IR}$ (mm)	2.98	2.99	3.02	3.05
	MAG × $FWHM\text{-}SSP_{IR}$	3.37	3.56	3.81	4.06
	Ratio	1	1.057	1.129	1.210

Values of *Ratio* are ratio of the product of the FWHM-SSP and MAG in height of 50 cm to the product of the FWHM-SSP and MAG in each height.

"MAG at each bead height" (Table 5) indicated a nearly constant value with an experimental error of 5% as compared to the reference value when the bead height was 50 mm. We also observed a negative correlation between the FWHM-SSP and MAG, where changes in the FWHM-SSPs were significantly associated with the MAG at each bead height.

The FWHM-SSP increased when the COR was set to be higher than the bead, and the FWHM-SSP decreased when the COR was set to be lower than the bead (Fig. 8). These results show that the COR height setting and the apparent angular range of the bead are related. When the bead height is set to be lower than the COR, the apparent angular range of the bead was less than the set angular range; when the bead height was set to be greater than the COR, the apparent angular range of the bead was greater than the set value. In fact, as the arrangement of the bead was increased (decreased) in height by 50 mm increments from the COR height, the apparent angular range decreased (increased) by 2° increments (Fig. 14). Theoretically, the larger angular range in the

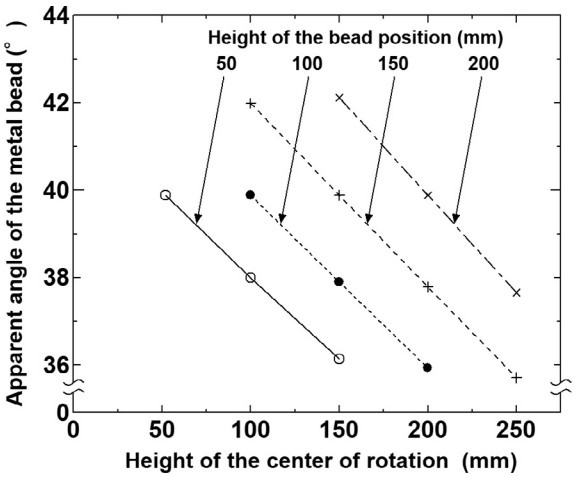

Fig. 14. Relationship between the COR setting and the apparent angle of the bead measured at various bead position from the table.

tomosynthesis system results in better resolution in the z direction. We believe that this theory was also applied to the apparent angular range of the beads in our results. At all bead heights, the apparent angular range and COR height had a negative correlation, and a certain change was found to have been exhibited. This shows that in tomosynthesis examinations performed over time in a clinical setting, tomosynthesis images with different the z resolution would be observed if the height of the anatomical structure of interest from the table, and the setting for the COR are not the same in the first and second/subsequent examinations. In other words, in comparative interpretations of tomosynthesis imaging, one must remember that the image comparison of the same z resolution is not possible if the height of the anatomical structure of interest from the table, and the setting for the COR are not the same.

The FWHM-SSP is greater with a small angular range for obtaining tomosynthesis images (Fig. 9). This is consistent with a past report [23] on conventional tomography and tomosynthesis. The rate of change in the FWHM-SSP measured at an angular range of 20°, and the rate of change in the FWHM-SSP measured at an angular range of 40° exhibited similar trends (Table 3). This result suggests that the change in the SSP when the bead and the COR heights have different settings is not a phenomenon observed only at an angular range of 40°, but rather at other angular ranges as well. The measurement results for the FWHM-SSP herein show that the FWHM-SSP can be estimated if the magnification rate or apparent angle of the bead used to measure the FWHM-SSP is calculated. Though the z resolution varies depending on the angular range and the design of the reconstruction filters, the quantitative knowledge about the changes in the SSP shown herein is useful for interpreting images with tomosynthesis imaging. It will also be useful in understanding and managing system properties.

The changes in the ASF were observed in all filters and at various height settings. The FWHM-ASF demonstrated a similar trend as the change of the FWHM-SSP. In this study, the SSP were also measured from the profile curve of the bead in the z direction relative to the table using images that were obtained at the center of the irradiation field. Therefore, the blurred effect can be observed in the z direction to the table for both SSP and ASF. In previous studies on digital breast tomosynthesis [25,26], the ASF has been evaluated using larger diameter bead than that used in this study. In addition, the ASF is reported to be affected by the diameter of the bead used [26]. Our results indicated a consistent trend with those of previous studies. In evaluating artifacts caused by large metals objects, further investigation may be necessary in the future.

The reported methods for measuring the SSP in tomosynthesis imaging include not only the method using a bead that we have used herein, but also methods using a metal wire or metal edge [24–26,31]. The methods with a wire or edge entail calculating the SSP from the measured values of the length of the wire or edge images. These measured values reportedly exhibit values lower by several percent than those from the technique herein with a bead [31]. Measurements of the SSP with tomosynthesis imaging obtained with a wire or edge would therefore exhibit smaller values than the results shown herein. However, because the rate of change in the FWHM-SSP with FBP is dependent on the apparent angular range and the magnification rate, as associated with differences in bead and COR heights, the results would be similar to the results shown herein.

This paper shows the differences in the rendering of phantom images in the quantitative measurement results for the SSP presented by tomosynthesis imaging, and describes the importance of understanding them. Tomosynthesis can provide in-depth information regarding structures of interest that cannot be indicated using 2D imaging. Moreover, the radiation dose in tomosynthesis was approximately a factor of 10 lower compared to the dose in the corresponding CT examinations [32]. In addition, if we can further understand the characteristics of the tomosynthesis images, it is evident that tomosynthesis imaging exhibits the potential to be a more useful examination for diagnostic imaging than ever.

The present study has some limitations: First, the study does not investigate other systems developed by different manufacturers. Properties pertaining to the SSP can be expected to also depend on the system algorithms. Strictly speaking, the results shown herein may not be indicative of the general features of tomosynthesis systems. Therefore, additional systematic research using other tomosynthesis systems needs to be conducted. However, to our knowledge, only a small number of manufacturers produce tomosynthesis systems with the ability to change the COR height used in our research; therefore, it may be very difficult to compare with other manufacturers' systems. Moreover, the large number of users worldwide who uses the tomosynthesis systems capable of the COR changes used in the present study means that the findings in this paper will be useful. The second limitation is that the SSP was not evaluated with measurements using beads of different materials than stainless steel. Changing the bead material may result in different the SSP, depending on the extent of the artifacts generated from the bead. Further investigations will need to be conducted with different materials, as well. The third limitation is that the quality of the reconstructed image for IR may depend on parameters. The IR used in this study does not possess characteristic of metal artifact reduction using metal extraction. In this study, the number of iterations was set to 4, which is often used in clinical practice. We have not yet evaluated the effect of the number of iterations in this study because our research is not intended to optimize the number of iterations. Another limitation of this study is that no comparison has been made between the experimental results and the simulation.

5. Conclusion

The SSP of the tomosynthesis system changed depending on the combination of the COR height and the height from the table used for evaluation (i.e., the bead height). This change was confirmed in anthropomorphic phantom images of bones and soft tissues. These results are anticipated to provide useful information for understanding the z resolution in tomosynthesis systems for an accurate diagnosis by radiologists, and in proper device management by device users.

Formatting of funding sources

This research did not receive any specific grant from funding agencies in the public, commercial, or not-for-profit sectors.

Acknowledgments

The authors are grateful to Takeshi Shiomi, Yukio Sato, Yuki Akagawa (Shimadzu Corporation), Yutaka Yoshida (Junshin Gakuen University) and Hiroshi Akamine (Kyushu University Hospital) for useful discussions. The authors thank the staff of the Division of Radiology at Kyushu University Hospital for their valuable clinical support.

References

[1] Dobbins III JT, Godfrey DJ. Digital x-ray tomosynthesis: current state of the art and clinical potential. Phys Med Biol 2003;48(19):R65–106.
[2] Grant DG. Tomosynthesis: a three-dimensional radiographic imaging technique. IEEE Trans Bio Eng 1972;1:20–8.
[3] Ziedses des Plantes BG. Eine neue method zur differenzierung in der roentgenographie (planigraphie). Acta Radiol 1932;13:182–92.
[4] Dobbins III JT. Tomosynthesis imaging: at a translational crossroads. Med Phys 2009;36(6):1956–67.
[5] Sabol JM. A Monte Carlo estimation of effective dose in chest tomosynthesis. Med Phys 2009;36(12):5480–7.
[6] Bath M, Svalkvist A, von Wrangel A, Rismyhr-Olsson H, Cederblad A. Effective dose to patients from chest examinations with tomosynthesis. Radiat Prot Dosimetry 2010;139(1–3):153–8.
[7] Nosratieh A, Yang K, Aminololama-Shakeri S, Boone JM. Comprehensive evaluation of the slice sensitivity profiles in breast tomosynthesis and breast CT. Med Phys 2012;39(12):7254–61.
[8] Sechopoulos I. A review of breast tomosynthesis. Part I. The image acquisition process. Med Phys 2013;40(1).
[9] Sechopoulos I. A review of breast tomosynthesis. Part II. Image reconstruction, processing and analysis, and advanced applications. Med Phys 2013;40(1).
[10] Johnsson AA, Fagman E, Vikgren J, Fisichella VA, Boijsen M, Flinck A, et al. Pulmonary nodule size evaluation with chest tomosynthesis. Radiology 2012;265(1):273–82.
[11] Johnsson AA, Svalkvist A, Vikgren J, Boijsen M, Flinck A, Kheddache S, et al. A Phantom study of nodule size evaluation with chest tomosynthesis and computed tomography. Radiat Prot Dosimetry 2010;139(1–3):140–3.
[12] Vikgren J, Zachrisson S, Svalkvist A, Johnsson AA, Boijsen M, Flinck A, et al. Comparison of chest tomosynthesis and chest radiography for detection of pulmonary nodules: human observer study of clinical cases. Radiology 2008;249(3):1034–41.
[13] Jung HN, Chung MJ, Koo JH, Kim HC, Lee KS. Digital tomosynthesis of the chest: utility for detection of lung metastasis in patients with colorectal cancer. Clin Radiol 2012;67(3):232–8.
[14] Canella C, Philippe P, Pansini V, Salleron J, Flipo RM, Cotten A. Use of tomosynthesis for erosion evaluation in rheumatoid arthritic hands and wrists. Radiology 2011;258(1):199–205.
[15] Duryea J, Dobbins III JT, Lynch JA. Digital tomosynthesis of hand joints for arthritis assessment. Med Phys 2003;30(3):325–33.
[16] Aoki T, Fujii M, Yamashita Y, Takahashi H, Oki H, Hayashida Y, et al. Tomosynthesis of the wrist and hand in patients with rheumatoid arthritis: comparison with radiography and MRI. Am J Roentgen 2014;202(2):386–90.
[17] Becker AS, Martini K, Higashigaito K, Guggenberger R, Andreisek G, Frauenfelder T. Dose reduction in tomosynthesis of the Wrist. Am J Roentgen 2017;208(1):159–64.
[18] Fahey FH, Webber RL, Chew FSK, Dickerson BA. Application of TACT to the evaluation of total joint arthroplasty. Med Phys 2003;30(3):454–9.
[19] Gomi T, Sakai R, Goto M, Hara H, Watanabe Y, Umeda T. Evaluation of digital tomosynthesis reconstruction algorithms used to reduce metal artifacts for arthroplasty: a phantom study. Phys Med 2017;42:28–38.
[20] Maltz JS, Fuerst J, Paidi A, Fadler F, Bani-Hashemi AR, Sprenger F. Fixed gantry tomosynthesis system for radiation therapy image guidance based on a multiple source x-ray tube with carbon nanotube cathodes. Med Phys 2009;36(5):1624–36.
[21] Machida H, Yuhara T, Mori T, Ueno E, Moribe Y, Sabol JM. Optimizing parameters

for flat-panel detector digital tomosynthesis. Radiographics 2010;30(2):549–62.
[22] Wu T, Moore RH, Rafferty A, Kopans DB. A comparison for reconstruction algorithms for breast tomosynthesis. Med Phys 2004;31(9):2636–47.
[23] Hu YH, Zhao B, Zhao W. Image artifacts in digital breast tomosynthesis: investigation of the effects of system geometry and reconstruction parameters using a linear system approach. Med Phys 2008;35(12):5242–52.
[24] Li B, Avinash GB, Eberhard JW, Claus BEH. Optimization of slice sensitivity profile for radiographic tomosynthesis. Med Phys. 2007;34(7):2907–16.
[25] Rodríguez-Ruiz A, Castillo M, Garayoa J, Chevalier M. Evaluation of the technical performance of three different commercial digital breast tomosynthesis systems in the clinical environment. Phys Med 2016;32(6):767–77.
[26] Maldera A, De Marco P, Colombo PE, Origgi D, Torresin A. Digital breast tomosynthesis: dose and image quality assessment. Phys Med 2017;33:56–66.
[27] European Reference Organisation for Quality Assured Breast Screening and Diagnostic Services (EUREF). Protocol for the quality control of the physical and technical aspects of digital breast tomosynthesis systems. Version 1.01. 2016 < http://www.euref.org/downloads?download=53:european-tomo-qc-protocol-version-1-01 > [accessed 12/28/2017].
[28] Burch A, Loader R, Rowberry B, Strudley C, Whitwam D. Routine quality control tests for breast tomosynthesis (physicists). National Health Services Breast Screening Program Equipment Report 2015; 1407 < https://www.gov.uk/government/uploads/system/uploads/attachment_data/file/488949/Breast_screening_1407_Physics_Tomo_QC_Protocol_Final_291215.pdf > [accessed 12/20/2017].
[29] Yaffe M, Maki A, Mawdsley G, Shen S, Mainprize J, Frimeth J. Quality assurance program for Tomosynthesis Imaging Screening Trial (TMIST). Draft document online 2015. < https://yaffegrp.sri.utoronto.ca/Physics/Physics_Manuals/TMIST_QC%20Manual_2015April15.pdf > [accessed 12/20/2017].
[30] Fukui R, Ishii R, Kishimoto J, Yamato S, Takahata A, Kohama C. Evaluation of the effect of geometry for measuring section thickness in tomosynthesis. Radiol Phys Technol 2014;7(1):141–7.
[31] Ikeno K, Akita T, Hanai K, Muramatsu Y. Investigation of the section thickness measurement in tomosynthesis by thin metal plate edge method. Jpn J Radiol Technol 2017;73(10):1007–17.
[32] Koyama S, Aoyama T, Oda N, Yamauchi-Kawaura C. Radiation dose evaluation in tomosynthesis and C-arm cone-beam CT examinations with an anthropomorphic phantom. Med Phys 2010;37(8):4298–306.
[33] Sakimoto T, Nishino K. Metal artifact reduction in tomosynthesis by metal extraction and ordered subset-expectation maximization (OS-EM) reconstruction. In: SPIE Med Imag; 2013: Int Soc Optics Photo. 2013; 86685M-86685M-86688.